Proceedings of ERAD (2002): 206–211 © Copernicus GmbH 2002

ERAD 2002

Determination of quality–controlled three–dimensional wind–vector fields using a bistatic Doppler radar

K. Friedrich and M. Hagen

Institut für Physik der Atmosphäre, DLR Oberpfaffenhofen, 82230 Wessling, Germany

Abstract. Horizontal wind–vector fields can be measured in real–time by a bistatic Doppler radar network and can be applied directly for hazard warnings and weather surveillance. But most applications especially for meteorological research and operational meteorology require quality–controlled wind–fields. Therefore, a quality–control scheme is developed which includes algorithms to determine the data quality by measured or fixed parameters. The algorithms are applied in the fuzzy logic sense weighting the quality of wind measurement with values ranging from one to zero. The results of each weighting algorithm are merged to an average quality–index field which represents the confidence of each horizontal wind measurement. This averaged field is available together with the measured horizontal wind–vector field for further applications. An overview about the determination and the quality control of three–dimensional wind–fields is presented for two frontal passages with stratiform precipitation and a convective situation.

1 Motivation

The bistatic Doppler radar system is an instrument capable of measuring simultaneously several components of the wind–vector which can be combined to a horizontal wind–vector field in real–time (Wurman et al., 1993). Several receivers separated spatially from the transmitter are implemented around the monostatic Doppler radar. Temporally and spatially high–resolution horizontal wind–vector fields are superior to one–dimensional radial Doppler velocity fields especially for detection of wind signatures for hazard warnings at airports, around populated areas, and for regional weather surveillance. Horizontal wind–vector fields are better and faster to interpret by everybody than one–dimensional radial Doppler velocity fields. But horizontal wind–fields can also be used for diagnostic research studies, now–casting of regional weather phenomena, and assimilation into numerical weather prediction models. For those application especially for operational usage, the confidence of the horizontal wind field estimation has to be analyzed by an automatically–working quality–control scheme. In this paper elements of the quality–control scheme are introduced which considers the signal quality, the influence of fixed parameters, the probability of contamination induced by the weather situation, and the data consistency in time and space.

Correspondence to: K. Friedrich (Katja.Friedrich@dlr.de)

2 The bistatic Doppler radar network

The bistatic Doppler radar network in Oberpfaffenhofen (OP) consists of the monostatic polarimetric Doppler radar system, POLDIRAD (Schroth et al., 1988), and three bistatic receivers at remote sites each containing both at least one antenna and a signal processor. In Fig. 1, the location of the three bistatic receivers and the respective look angles of the bistatic antennas are illustrated. The investigation area, indicated schematically, is restricted by the received power pattern of the bistatic antenna, which has a horizontal angular aperture covering about -30° to 30°. The horizontal antenna aperture together with range arcs are exhibited in Fig. 1 for each bistatic antenna.

Both receiver systems at Lagerlechfeld and Lichtenau are equipped with two antennas each, which have a vertical angular aperture covering 1° to 9° for measurements within the boundary layer and 1° to 23° for measuring thunderstorms, respectively. At Ried, one antenna having a vertical aperture of 8° has been installed. At the moment, the bistatic radar network at OP covers an area of about 50 km $\times$ 50 km. Within this area, horizontal wind–fields are determined exactly in the dual–Doppler area (in Fig. 1 hatched) and overdetermined in triple–/quadruple–Doppler areas (in Fig. 1 cross–hatched).

Due to a limited vertical antenna aperture of 8° oriented close to the ground, the measured wind components are dominated by the horizontal components u, v. As a result, these measurements are used only to determine the horizon-

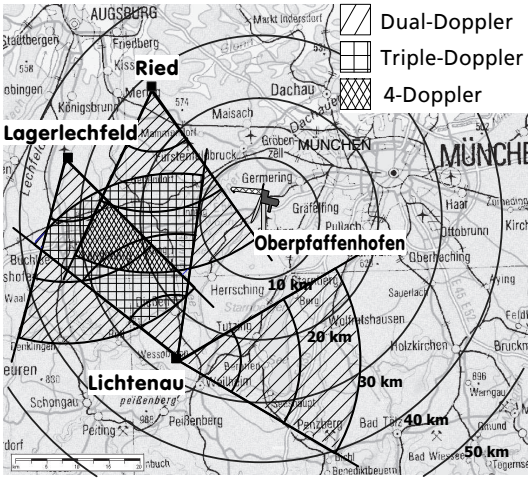

Fig. 1. Map of the bistatic multiple-Doppler radar network at the DLR in OP consisting of POLDIRAD and three bistatic receivers located at Lichtenau, Lagerlechfeld, and Ried. The investigation area is restricted by the horizontal antenna aperture of the bistatic antennas. The equation system to calculated the horizontal wind–field is exactly determined in the dual-Doppler areas (hatched) and overdetermined in the triple- or quadruple–Doppler areas (cross-hatched). More explanations in the text.

tal wind–vector field directly. The vertical component, w, is retrieved by means of a variational analysis method (Protat and Zawadzki, 1999).

3 The quality–control scheme

3.1 The decision criterion based on the signal quality

At the remote receiver the velocity–power spectrum is obtained. The power, Doppler velocity, and normalized coherent power[1] (NCP) are transfered to the central hub computer located at OP, where the data of all receivers is collected, the horizontal wind–field is determined and quality–controlled.

At the central bistatic hub computer, first data with large velocity dispersion and low reflectivity factors are rejected using an empirically chosen threshold of NCP ≤ 0.3.

As an example of applying the NCP criterion on measured data, Fig. 2 presents a horizontal cross–section at 1.6 km above MSL of the horizontal wind–vector field superimposed on the bistatic reflectivity factor, Z_b, measured by the bistatic receiver Lagerlechfeld. In Figure 2a the NCP criterion is not applied, while in Fig. 2b noisy data is removed using the NCP criterion.

3.2 The quality–index fields

The following algorithms are applied in the fuzzy logic sense weighting the quality with values ranging from zero to one. The results of each weighting algorithm can be merged to

[1]Index related inversely to the spectral width ranging from zero to one (for more details see (Friedrich, 2002)).

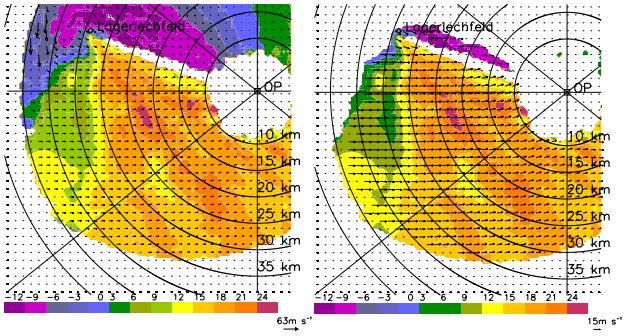

Z_b[dBZ] **(a)** Z_b[dBZ] **(b)**

Fig. 2. Horizontal cross–section at 1.6 km above MSL of the horizontal wind in $\mathrm{m\,s^{-1}}$ (arrows) underlaid by the bistatic reflectivity factor field, Z_b, in dBZ measured by the receiver Lagerlechfeld on 2 February 2000 at 17:08 UTC (a) without applying the NCP criterion and (b) with applying the NCP criterion on the measured data. The horizontal wind–vector is determined by using the Doppler velocity sampled by receivers Lagerlechfeld and OP.

achieve an average quality–control field which reflects the confidence of each horizontal wind measurement. All thresholds are set empirically.

In the following sections, three quality–index fields are defined according to: (1) the accuracy of the horizontal wind–field depending on the location of transmitter, target, and receiver, denoted as $F(\sigma'_{|\mathbf{V}_h|})$; (2) the probability of side-lobe contamination, denoted as $F(\nabla Z)$; and (3) the fractional uncertainty of the wind–field measurement, denoted as $F(\sigma'_{|\mathbf{V}_h|}/|\mathbf{V}_h|)$. Note that the standard deviation of the horizontal wind–field, induced by the position of transmitter, target, and receivers, is fixed for a chosen experimental setup.

The influence of each quality–index field on the average quality–index field can be chosen according to the application of those quality–controlled wind–vectors and the weather situation with the respective weights $W_{F(\sigma'_{|\mathbf{V}_h|})}, W_{F(\nabla Z)}$, and $W_{F(\sigma'_{|\mathbf{V}_h|}/|\mathbf{V}_h|)}$. $W_{F(v_r/v_t)}$. The quality fields can then be averaged to a single quality field using

$$\bar{F} = \frac{1}{C}\Big(W_{F(\sigma'|\mathbf{V}_h|)}F(\sigma'_{|\mathbf{V}_h|}) + W_{F(\nabla Z)}F(\nabla Z) + W_{F(\sigma'_{|\mathbf{V}_h|}/|\mathbf{V}_h|)}F(\sigma'_{|\mathbf{V}_h|}/|\mathbf{V}_h|)\Big), \quad (1)$$

where

$$C = W_{F(\sigma'|\mathbf{V}_h|)} + W_{F(\nabla Z)} + W_{F(\sigma'_{|\mathbf{V}_h|}/|\mathbf{V}_h|)} \quad .$$

Each quality–index field and the average index field range between zero and one.

3.2.1 Utilizing geometrical accuracy

The horizontal wind–field is determined by the velocity components measured by the monostatic and bistatic receiver.

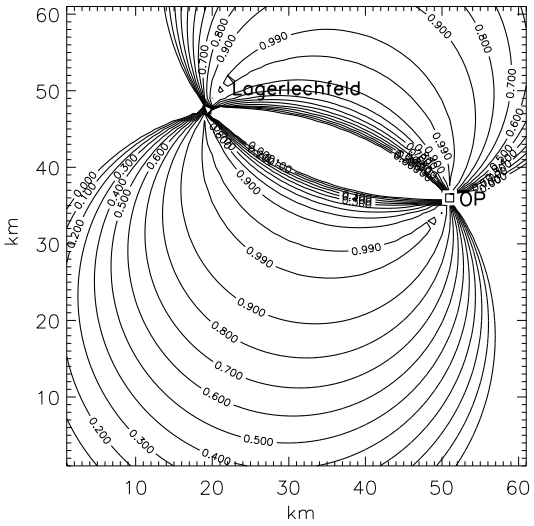

Fig. 3. Horizontal cross–section at ground level of the quality–index field $F(\sigma'_{|\mathbf{V}_h|})$ for the bistatic dual–Doppler radar system consisting of OP and Lagerlechfeld.

The standard deviation of the horizontal wind–field depends on the intersection angle between the two velocity components. The highest accuracy is achieved at an intersection angle of about 50°. Horizontal wind–fields can not be determined at intersection angles of 0° and 90°, respectively (Friedrich, 2002). The standard deviation of the horizontal wind–field can be expressed by the quality–index field $F(\sigma'_{|\mathbf{V}_h|})$. Only the geometrical location of transmitter, receiver, and target is considered.

For a dual–Doppler radar system, the highest accuracy in the horizontal wind–field determination is expressed by $F(\sigma'_{|\mathbf{V}_h|})$ = 1 at $\min(\sigma'_{|\mathbf{V}_h|})$ and lowest accuracy by $F(\sigma'_{|\mathbf{V}_h|})$ = 0. Due to the infinity of $\sigma'_{|\mathbf{V}_h|}$ close to the baseline, the upper limit of $\sigma'_{|\mathbf{V}_h|}$ ($\max(\sigma'_{|\mathbf{V}_h|})$ has to be chosen empirically. For a bistatic dual–Doppler radar system, the standard deviation reaches its minimum at a intersection angle of about 50° with $\min(\sigma'_{|\mathbf{V}_h|})$ = 2.42, and $\max(\sigma'_{|\mathbf{V}_h|})$ set empirically to 5.0 (the values are normalized by the standard deviation of Doppler velocity measurement achieved by a monostatic radar which is assumed to be 1 $\mathrm{m\,s^{-1}}$). The definition of $F(\sigma'_{|\mathbf{V}_h|})$ is given by

$$F(\sigma'_{|\mathbf{V}_h|}) = \frac{\max(\sigma'_{|\mathbf{V}_h|}) - \sigma'_{|\mathbf{V}_h|}}{\max(\sigma'_{|\mathbf{V}_h|}) - \min(\sigma'_{|\mathbf{V}_h|})}. \quad (2)$$

A horizontal cross–section of the distribution of the quality–index field $F(\sigma'_{|\mathbf{V}_h|})$ for the bistatic dual–Doppler radar system (POLDIRAD + Lagerlechfeld) is shown in Fig. 3.

3.2.2 Utilizing signal quality based on the reflectivity gradient

In this section, the probability of contamination caused by the weather situation on the measurements is investigated. Data measured by a bistatic receiver is more likely to be contaminated by sidelobes of the transmitted radar due to the wide–beam receiving antennas (more details by de Elia and Zawadzki (1999); Friedrich (2002)). For narrow–beam antennas, sidelobe contamination can be ignored, because the signal transmitted through the weak sidelobe is also received by the weak sidelobe. Therefore, the reflectivity factor measured by the monostatic radar can be used as a reference to give information about the probability of sidelobe contamination.

The probability that data measured by the bistatic receiver is contaminated by sidelobes of the transmitted antenna pattern can be expressed by the gradient of the reflectivity factor, $\nabla Z = (\frac{\partial Z}{\partial x}, \frac{\partial Z}{\partial y}, \frac{\partial Z}{\partial z})$. The absolute value of the reflectivity factor gradient can be expressed by the quality–field $F(\nabla Z)$ with

$$F(\nabla Z) = \left(30\text{dBZ/km} - \sqrt{\left(\frac{\Delta Z}{2\Delta x}\right)^2 + \left(\frac{\Delta Z}{2\Delta y}\right)^2 + \left(\frac{\Delta Z}{2\Delta z}\right)^2} \right) / \left(30\text{dBZ/km} \right). \quad (3)$$

The upper–limit value of 30 dBZ/km is derived from the beam pattern of the transmitting antenna at POLDIRAD (Fig. 2.11 in Friedrich, 2002). Here, the first sidelobe of the transmitted beam pattern occurs at about 1.7° away from the main beam, with a reduction of about 32 dB when compared to the mainlobe. Thus, assuming a uniform receiving beam pattern of the bistatic antenna, the gradient of the reflectivity factor has to be about 30 dBZ per 1.7° in order to measure the same signal intensity from the sidelobe as that obtained from the mainlobe by the bistatic receiver.

At $F(\nabla Z)$ = 0, the probability of sidelobe contamination is very high, while at $F(\nabla Z)$ = 1, sidelobe contamination hardly occurs. As an example, the horizontal distribution of $F(\nabla Z)$ is analyzed in Fig. 4 for the reflectivity factor field of a convective cell. The impact of $F(\nabla Z)$ on the averaged quality–index field is set by the weighting factor $W_{F(\nabla Z)}$.

3.2.3 Utilizing signal quality based on fractional uncertainty

The fractional uncertainty field, $\sigma'_{|\mathbf{V}_h|}/|\mathbf{V}_h|$, is used to give information about the percentage accuracy of the horizontal wind–field measurement. The quality–index field $F(\sigma'_{|\mathbf{V}_h|}/|\mathbf{V}_h|)$, related to the wind–field variability, is derived linearly from $\sigma'_{|\mathbf{V}_h|}/|\mathbf{V}_h|$ using

$$F(\sigma'_{|\mathbf{V}_h|}/|\mathbf{V}_h|) = \begin{cases} 1 - \frac{\sigma'_{|\mathbf{V}_h|}}{|\mathbf{V}_h|} & \text{for } \sigma'_{|\mathbf{V}_h|} < |\mathbf{V}_h| \\ 0 & \text{for } \sigma'_{|\mathbf{V}_h|} \geq |\mathbf{V}_h| \end{cases}. \quad (4)$$

For $\sigma'_{|\mathbf{V}_h|} \ll |\mathbf{V}_h|$, $F(\sigma'_{|\mathbf{V}_h|}/|\mathbf{V}_h|)$ approaches the value of one. Figure 5 shows the horizontal distribution of $F(\sigma'_{|\mathbf{V}_h|}/|\mathbf{V}_h|)$ for the simulated convective cell. The horizontal wind–field of the simulated supercell storm (Fig. 5a) is used to calculate $F(\sigma'_{|\mathbf{V}_h|}/|\mathbf{V}_h|)$ for the dual–Doppler configuration consisting of POLDIRAD and receiver Lagerlechfeld. Because the wind–velocity measurement is an

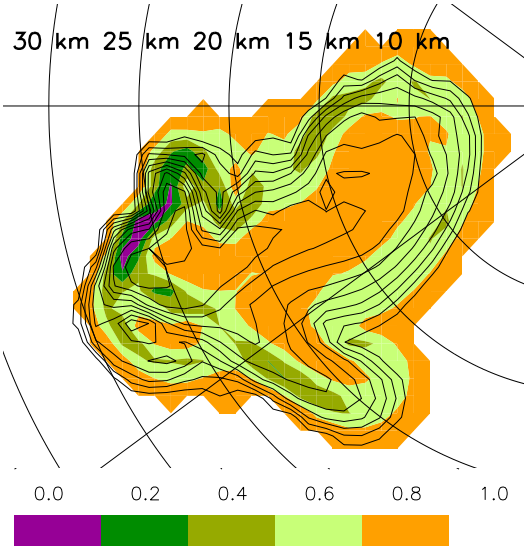

Fig. 4. Horizontal cross–section of $F(\nabla Z)$ (color–coded) calculated for a convective cell. The isolines indicating the gradient of reflectivity factor are plotted every 5 dBZ starting at the outside of the cell with the 5 dBZ–isoline.

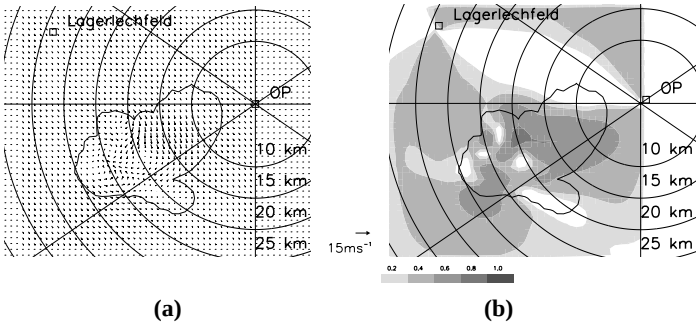

Fig. 5. Horizontal cross–section of (a) the horizontal wind–vector of the simulated convective cell and (b) the respective quality–index field $F(\sigma'_{|\mathbf{V}_h|}/|\mathbf{V}_h|)$. The 5 dBZ–isoline indicating the shape of the supercell storm is marked.

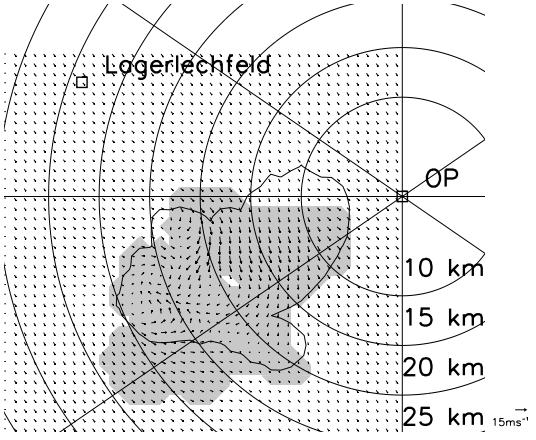

Fig. 6. Horizontal cross–section of the horizontal wind–vector in $\mathrm{m\,s^{-1}}$ a convective storm. The area with wind–shear (direction and absolute value) higher than mean flow is marked. The 5 dBZ–isoline indicating the shape of the storm is marked.

absolute measurement, low wind–speeds create low values of $F(\sigma'_{|\mathbf{V}_h|}/|\mathbf{V}_h|)$. In addition, high standard deviations, e.g. close to the baseline or in the quasi–monostatic area, cause low values of $F(\sigma'_{|\mathbf{V}_h|}/|\mathbf{V}_h|)$. The influence of $F(\sigma'_{|\mathbf{V}_h|}/|\mathbf{V}_h|)$ on the average quality–control field is controlled by the weight of $W_{F(\sigma'_{|\mathbf{V}_h|}/|\mathbf{V}_h|)}$.

The weight of this quality–index field on the average quality–index field should be set low within those weather conditions having high wind–shear. For example, as illustrated in Fig. 5b at an azimuth angle of $200° \leq \phi_t \leq 225°$ and at a range of r'_t = 20 km – 25 km, the wind–speed is very weak and causes $F(\sigma'_{|\mathbf{V}_h|}/|\mathbf{V}_h|)$ to be close to zero, even though $\sigma'_{|\mathbf{V}_h|}$ is low and the wind represents realistic conditions within this area. To avoid a wrong interpretation of $F(\sigma'_{|\mathbf{V}_h|}/|\mathbf{V}_h|)$, $W_{F(\sigma'_{|\mathbf{V}_h|}/|\mathbf{V}_h|)}$ should be set high during stratiform precipitation with wind–speed values larger than 5 $\mathrm{m\,s^{-1}}$ and low during situations with high wind–shear, e.g. convective situations.

The fractional uncertainty can also be applied to the direction of the horizontal wind.

3.2.4 Utilizing data consistency based on a persistence check

The persistence check algorithm should help in identifying regions where wind–shear is higher than the mean flow. The regions identified are then tracked in space by means of wind–fields at different elevations and at different time steps (e.g. successive volume–scans). When high wind–shear is identified at different levels and/or in the successive volume–scans, the wind–shear can be related to atmospherical processes. Otherwise, the perturbation is removed.

The persistence check is carried out as follows. The standard deviation in the horizontal wind–velocity, $\sigma_{|\mathbf{V}_h|}$, and direction are calculated. The area is marked, when the difference between the mean value, $\overline{\mathbf{V}_h}$, minus the $i'th$ measured horizontal wind–vector, $\mathbf{V}^i$ is larger than the vector standard deviation, $\sigma_{\mathbf{V}_h}$. For the horizontal wind–velocity this is given as

$$\sigma_{|\mathbf{V}_h|} - |\overline{\mathbf{V}_h} - \mathbf{V}^i| \leq 0 \quad . \tag{5}$$

Figure 6 shows an example of how this algorithm is applied using the horizontal wind–field of a convective storm. The shape of the supercell storm is indicated by the 5 dBZ–isoline. The wind–shear within the storm is much higher than the surrounding air flow. Therefore, the area having high wind–shear is marked. Note that if the area marked gray is present in the successive volume scans as well as at neighboring levels, the marked area can then be identified as a signal which is related to meteorological processes. Otherwise, wind–vectors within this area will be removed.

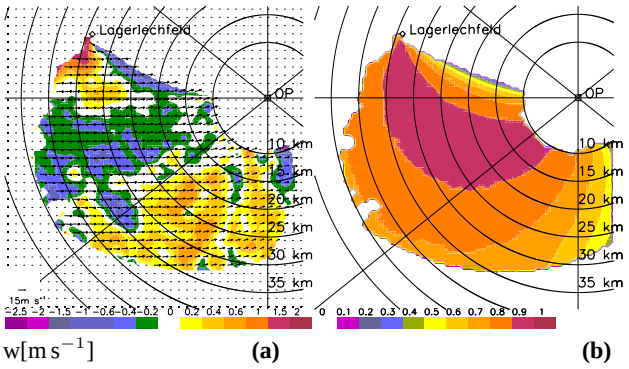

Fig. 7. Horizontal cross–section at a height of 1.6 km above MSL of the (a) retrieved horizontal wind–vector underlaid by vertical velocity in m s^{-1} and (b) the respective quality–index field of the horizontal wind on 2 February 2000 at 17:08 UTC. Updraft motions are indicated by positive values, and downdraft by negative values. For clarity of display, only every third wind vector is plotted.

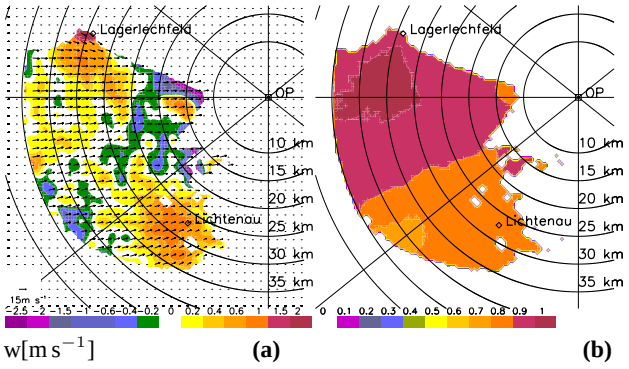

Fig. 8. As Fig. 7, for 10 April 2001 at 13:27 UTC. Data were sampled by the receivers Oberpfaffenhofen, Lichtenau, and Lagerlechfeld.

4 Stratiform precipitation in a frontal system

Two cold frontal systems with stratiform precipitation passed over southern Germany from the northwest on 2 February 2000 and 10 April 2001, respectively. On both days the pre–frontal wind was mainly from southwesterly and westerly directions, ranging from between 10 m s^{-1} – 15 m s^{-1} and increasing and veering more to a westerly flow as the cold front approached. On 2 February 2000 data was measured by POLDIRAD and the receiver Lagerlechfeld . On 10 April 2001 the bistatic Doppler radar network consisted of POLDIRAD, receiver Lagerlechfeld, and receiver Lichtenau. Both data sets were interpolated onto a Cartesian grid with a horizontal resolution of 500 m and a vertical resolution of 250 m, starting at 600 m above MSL, i.e. at the height of POLDIRAD, up to a height of 2.85 km above MSL. The measured velocities, v_t and v_e, were used as input data for the constraining model (Protat and Zawadzki, 1999) in order to retrieve the three components, u, v, w of the wind–vector.

Figure 7a shows the horizontal wind–vector underlaid by the vertical velocity during the frontal passage on 2 February 2000 at 17:08 UTC. The frontal system was located SW of OP (between $220° \leq \phi_t \leq 230°$), heading southeast. In Fig. 7a, a perturbation can be detected SW of OP with a slight change in wind direction (from SW to W), with pre–frontal ascending and post–frontal descending air. The averaged quality–index field of the horizontal wind–vector at 17:08 UTC is exhibited in Fig. 7b. In this case, which shows a weather situation with a relatively homogeneous flow, the quality–index field is dominated by the accuracy of the horizontal wind–field determination (cp. Fig. 5). Only wind–vector and values of reflectivity factor where the average quality–index field exceeded a value of 0.6 (empirically chosen) were plotted. Within this area, the confidence in the Doppler velocity measurements was high, and a large number of data points was available.

Figure 8 illustrates the vertical wind–field superimposed on the horizontal wind–vector field, and the corresponding average quality–index field of the horizontal wind on 10 April 2001 at 13:27 UTC, respectively. The influence of an overdetermined equation system for the horizontal wind–field calculation on the averaged quality index field can be seen clearly when comparing Fig. 7b and Fig. 8b. According to the quality–index field (Fig. 8b), the confidence in the horizontal wind–field is high within the whole observation area with values ranging between 0.7 and 0.8. The retrieved vertical velocity was characterized by relatively small up– and downward motions due to the low values of horizontal convergence.

5 Convective weather situation

On the afternoon of the 3 May 2000, a convective systems developed southwest of OP around 14:00 UTC and stayed within the observation area for one hour.

The most active part of the system located southwest of Oberpfaffenhofen (i.e. maximum reflectivity factor) consisted of a stationary cell located between $225° \leq \phi_t \leq 280°$ at a range of 15 km $\leq r'_t \leq$ 30 km. Volume scans were performed by POLDIRAD and receiver Lagerlechfeld.

Owing to the high variability in wind direction and speed, the weights for the quality index related to $F(\sigma'_{|\mathbf{V}_h|}/|\mathbf{V}_h|)$ were set to zero. Furthermore, $F(\nabla Z)$ showed a probability of sidelobe contamination because of the high gradient in the reflectivity factor. Sidelobe contamination was investigated separately. The results showed no contamination of data measured by the bistatic receiver during this convective situation (Friedrich, 2002). The confidence in the horizontal wind–field ranged between 0.5 and 0.8.

The wind–field retrieval was performed in a 40 km $\times$ 40 km $\times$ 10 km domain and interpolated onto a Cartesian grid with a horizontal and a vertical resolution of 500 m. The retrieval domain consisted of 20 height levels, beginning at 600 m and reaching up to a height of 10.6 km above MSL.

Figure 9 shows the retrieved horizontal wind–vector underlaid by the vertical velocity at 14:55 UTC at a height

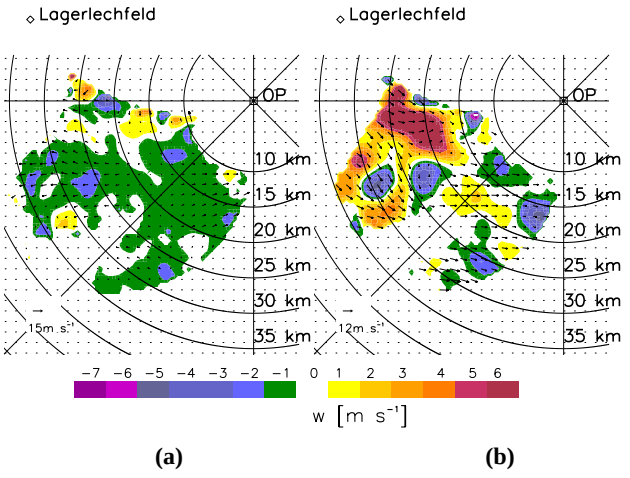

Fig. 9. Horizontal cross–section of the horizontal wind–vector in m s^{-1} at a height of (a) 1.35 km and (b) 5.35 km above MSL underlaid by the vertical velocity in m s^{-1} for 3 May 2000, at 14:55 UTC. The horizontal wind was determined by the Doppler measurements of receivers OP and Lagerlechfeld. Upwinds are indicated by positive values, while negative values are downwinds. For clarity of display, only every third wind–vector is plotted.

of 1.35 km and 5.35 km above MSL. The horizontal wind–vector at the lower troposphere showed strong divergences and convergences in speed and direction with an easterly and westerly flow at 1.35 km above MSL (Fig. 9a). Aloft, northwesterly to westerly winds dominated (Fig. 9b), with a noticeable confluence of the outflow on the southern part of the most active part of the system. The vertical velocity fields were characterized by a well–defined updraft located at $230° \leq \phi_t \leq 270°$at a range of 15 km $\leq r_t \leq$ 25 km and a downdraft area south of it. The magnitude of the up– and downdraft was continuously increasing from ground level up to the top. Maximum values of 6 m s^{-1} at a height of 5.35 km above MSL were reached in the updraft region and values of -5 m s^{-1} at 5.35 km above MSL in the southern downdraft region (Fig. 9b). Both positive and negative divergences of the horizontal wind–field were observed in the main updraft area.

6 Conclusion

Signatures of the horizontal wind–field (e.g. divergences, rotations, wind–shear) can be detected easily with a bistatic Doppler radar as presented here for two stratiform and one convective precipitation event. While the horizontal wind is measured in real–time, the quality–control and the vertical wind retrieval are applied afterwards. The three components of the wind–vector u, v, and w together with a confidence level for each horizontal wind–field is a great benefit for operational meteorology, e.g. weather surveillance, hazard warnings, and nowcasting of weather phenomena.

The comprehensiveness and the emphasis to the quality–control scheme varied according to the weather situations. During the stratiform precipitation event, for instance, the quality of horizontal wind is dominated by $F(\sigma'_{|\mathbf{V}_h|})$ which is fixed for an experimental setup. Low impact is observed by $F(\nabla Z)$ and $F(\sigma'_{|\mathbf{V}_h|}/|\mathbf{V}_h|)$. The emphasis on the quality control was set differently by the convective case. For instance, $F(\sigma'_{|\mathbf{V}_h|}/|\mathbf{V}_h|)$ could not be applied owing to the high wind–shear. On the other hand, the control for data consistency, such as the persistence check in time and space and investigation on sidelobe contamination, was more important. The cases discussed here show clearly that quality–control algorithms must be flexibly and independently applicable. The quality–control algorithm can also be applied to other horizontal wind–field measurements, e.g. monostatic dual–Doppler winds.

References

de Elia, R. and Zawadzki, I., Sidelobe contamination in bistatic radars, in Proc.29th Radar Meteorology Conf., Montreal, pp. 218–220, Amer. Meteor. Soc., 1999.

Friedrich, K., Determination of three–dimensional wind–vector fields using a bistatic Doppler radar network, Ph.D. thesis, Fakultaet fuer Physik, Ludwig–Maximilians–Universitaet Muenchen, http://www.op.dlr.de/ pa4k/, 2002.

Protat, A. and Zawadzki, I., A variational method for real–time retrieval of three–dimensional wind field from multiple–Doppler bistatic radar network data, J. Atmos. Oceanic Technol., 16, 432–449, 1999.

Schroth, A. C., Chandra, M. S., and Meischner, P., A C–band coherent polarimetric radar for precipitation and cloud physics research, J. Atmos. Oceanic Technol., 5, 803–822, 1988.

Wurman, J., Heckman, S., and Boccippio, D., A bistatic multiple–Doppler radar network, J. Appl. Meteor., 32, 1802–1814, 1993.